Bioorganic & Medicinal Chemistry Letters 20 (2010) 7004–7010

Contents lists available at ScienceDirect

Bioorganic & Medicinal Chemistry Letters

journal homepage: www.elsevier.com/locate/bmcl

3D-QSAR, homology modeling, and molecular docking studies on spiropiperidines analogues as agonists of nociceptin/orphanin FQ receptor

Ming Liu, Lin He, Xiaopeng Hu, Peiqing Liu, Hai-Bin Luo *

School of Pharmaceutical Sciences, Sun Yat-Sen University, Guangzhou 510006, PR China

ARTICLE INFO

Article history:
Received 3 May 2010
Revised 22 September 2010
Accepted 24 September 2010
Available online 29 September 2010

Keywords:
NOP
Agonist
3D-QSAR
CoMFA
Homology modeling
Molecular docking

ABSTRACT

The nociceptin/orphanin FQ receptor (NOP) has been implicated in a wide range of biological functions, including pain, anxiety, depression and drug abuse. Especially, its agonists have a great potential to be developed into anxiolytics. However, the crystal structure of NOP is still not available. In the present work, both structure-based and ligand-based modeling methods have been used to achieve a comprehensive understanding on 67 N-substituted spiropiperidine analogues as NOP agonists. The comparative molecular-field analysis method was performed to formulate a reasonable 3D-QSAR model (cross-validated coefficient $q^2 = 0.819$ and conventional $r^2 = 0.950$), whose robustness and predictability were further verified by leave-eight-out, Y-randomization, and external test-set validations. The excellent performance of CoMFA to the affinity differences among these compounds was attributed to the contributions of electrostatic/hydrogen-bonding and steric/hydrophobic interactions, which was supported by the Surflex-Dock and CDOCKER molecular-docking simulations based on the 3D model of NOP built by the homology modeling method. The CoMFA contour maps and the molecular docking simulations were integrated to propose a binding mode for the spiropiperidine analogues at the binding site of NOP.

The nociceptin/orphanin FQ receptor (NOP), also known as ORL1, OP4, or LC132, is a deorphanized member of the G-protein coupled receptor (GPCR) superfamily. This receptor is distributed in the brain and periphery.[1] It shares considerable structural and localization features with other opioid receptors,[2] but it is classified as a non-opioid member of the opioid receptor family by the International Union of Basic and Clinical Pharmacology (IUPHAR). Its endogenous ligand, nociceptin (or orphanin FQ), which activates NOP, is a 17-amino acid neuropeptide isolated from the brain in 1995.[3,4] The neuropeptide acts as an inhibitive agent on synaptic transmission in the CNS, and reduces responsiveness to stress. The nociceptin-NOP system has been implicated in a wide range of biological functions, including pain, mood disorders, drug abuse, cardiovascular control, and immunity.[5–7] NOP is receiving considerable attention as a potential target for the treatment of anxiety and depression.

A number of drugs are used for the treatment of anxiety and depression. But they have some drawbacks due to their poor and/or variable efficacy, long run in to peak behavioral effect, and a wide range of side effects leading to tolerability and compliance problems.[8] Considerable evidences indicate that nociceptin and several non-peptide NOP agonists serve as anxiolytics with fewer side effects.[9–17]

Several different classes of NOP agonists have been reported. Among them, spiropiperidine analogues exhibit relatively higher NOP binding affinities,[18,19] however, there is not a QSAR (quantitative structure–activity relationship) or pharmacophore model reported in their work. In the present study, comparative molecular-field analysis (CoMFA) was performed to formulate 3D-QSAR models of 67 spiropiperidine analogues[19] as NOP agonists. Subsequently, a homology model was build based on the crystal structure of Beta2-Adrenergic G Protein-Coupled receptor (PDB code: 2RH1)[20] as a template. Finally, molecular docking simulations were performed to obtain a complete picture of the structural characteristics of the most active agonist **P67** within the putative active site of this protein. Results of the study not only support the use of spiropiperidine analogues as a potential therapeutic agent by targeting NOP, but also aid the rational design of novel and more effective NOP agonists as desired.

Sixty-seven N-substituted spiropiperidine analogues with human NOP binding affinities (K_i) determined from competition binding assays were collected from the literature.[19] The 67 molecules were divided into a training set of 57 compounds and a test set of 10 compounds, as shown in Table 1. The test set covers the range of biological activities and indicates a moderate diversity in their chemical structures. The experimental pK_i values ($-\log K_i$) were used for the 3D-QSAR analysis.

The three-dimensional structures were constructed using SYBYL programming package (version 7.3.5).[21] The MMFF94 force field and MMFF94 partial atomic charges were applied to these

* Corresponding author. Tel.: +86 20 39943031.
E-mail address: luohb77@mail.sysu.edu.cn (H.-B. Luo).

0960-894X/$ - see front matter © 2010 Elsevier Ltd. All rights reserved.
doi:10.1016/j.bmcl.2010.09.116

Table 1
Structures, experimental,[19] and CoMFA-predicted activities of spiropiperidines analogues as nociceptin/orphanin FQ receptor (NOP) agonists

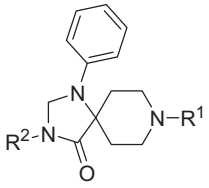

A
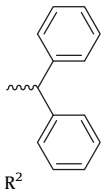

B
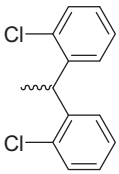

C
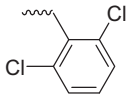

D
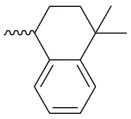

Compound	R^1	R^2	−log (K_i/nM)		
			Experimental	Predicted	Res
P09	A	H-	7.638	7.654	−0.016
P10[a]	A	Me	7.509	7.183	0.326
P11	A	Et	7.076	7.112	−0.036
P12	A	Pr	7.469	7.242	0.227
P13	A	Bu	7.244	7.344	−0.100
P14	A	*i*-Pr	7.180	7.242	−0.062
P15	A	*c*-PrCH$_2$	7.081	6.967	0.114
P16	A	*c*-BuCH$_2$	7.276	7.209	0.067
P17[a]	A	*c*-HexylCH$_2$	7.051	7.154	−0.103
P18	A	Propargyl	6.631	6.800	−0.169
P19	A	Allyl	6.693	6.750	−0.057
P02	B	H–	8.167	8.067	0.100
P20	B	Bu–	7.312	7.587	−0.275
P21	B	*i*-Amyl	7.252	7.476	−0.224
P22	B	CH$_3$OC(O)CH$_2$–	7.710	7.705	0.005
P23	B	HO(CH$_2$)$_2$	7.733	8.052	−0.319
P24	B	MeO(CH$_2$)$_2$	7.585	7.826	−0.241
P25[a]	B	NH$_2$(CH$_2$)$_2$–	7.321	7.621	−0.300
P26	B	CH$_3$NH(CH$_2$)$_2$–	8.393	8.274	0.119
P27	B	EtNH(CH$_2$)$_2$–	8.678	8.531	0.147
P28	B	*i*-PrNH(CH$_2$)$_2$–	8.593	8.376	0.217
P29	B	*c*-PentylNH(CH$_2$)$_2$–	8.063	8.395	−0.332
P30	B	*c*-HexylNH(CH$_2$)$_2$–	8.301	8.369	−0.068
P31	B	(CH$_3$)$_2$N(CH$_2$)$_2$–	8.456	8.138	0.318
P32	B	*c*-PrNH(CH$_2$)$_2$–	8.432	8.420	0.012
P33	B	(*i*-Pr)$_2$N(CH$_2$)$_2$–	7.917	7.802	0.115
P34[a]	B	BuNH(CH$_2$)$_2$–	8.668	8.662	0.006
P35	B	*i*-BuNH(CH$_2$)$_2$–	8.561	8.698	−0.137
P36	B	BuNH(CH$_2$)$_2$–	8.420	8.601	−0.181
P37	B	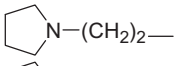	8.648	8.324	0.324
P38	B	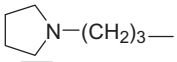	8.495	8.288	0.207
P39	B	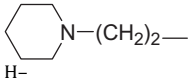	8.097	7.900	0.197
P40	C	H–	8.638	8.729	−0.091
P41	C	CH$_3$NH(CH$_2$)$_2$–	9.097	8.845	0.252
P42	C	EtNH(CH$_2$)$_2$–	9.155	9.167	−0.012
P43[a]	C	*i*-PrCH$_2$NH(CH$_2$)$_2$–	9.155	9.041	0.114
P44	C	*c*-PrCH$_2$NH(CH$_2$)$_2$–	9.301	9.470	−0.169
P45	C	*c*-BuNH(CH$_2$)$_2$–	9.301	9.048	0.262
P46	C	PrNH(CH$_2$)$_2$–	9.222	9.333	−0.111
P47	C	*i*-BuNH(CH$_2$)$_2$–	9.301	9.371	−0.070
P48	C	BuNH(CH$_2$)$_2$–	9.398	9.282	0.116
P49	C	Et$_2$N(CH$_2$)$_2$–	9.000	8.992	0.008
P50	C	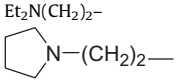	8.638	8.939	−0.301
P03	D	H–	8.886	8.538	0.348
P51[a]	D	Pr–	8.268	8.132	0.136
P52	D	CH$_3$C(O)CH$_2$–	8.347	8.541	−0.194
P53	D	HO(CH$_2$)$_2$–	8.770	8.602	0.098
P54	D	CH$_3$NH(CH$_2$)$_2$–	8.678	8.702	−0.024
P55	D	EtNH(CH$_2$)$_2$–	8.796	9.029	−0.233
P56[a]	D	*i*-PrNH(CH$_2$)$_2$–	8.854	8.970	−0.116
P57	D	*c*-PentylNH(CH$_2$)$_2$–	9.046	8.965	0.081
P58	D	*c*-HexylNH(CH$_2$)$_2$–	9.046	9.016	0.030
P59	D	PrNH(CH$_2$)$_2$–	9.000	9.204	−0.204
P60	D	CH$_2$=CHCH$_2$NH(CH$_2$)$_2$–	9.046	9.090	−0.044
P61	D	*c*-BuNH(CH$_2$)$_2$–	8.824	8.910	−0.086
P62	D	*c*-PrCH$_2$NH(CH$_2$)$_2$–	9.097	9.123	−0.026
P63	D	*i*-BuNH(CH$_2$)$_2$–	9.301	9.237	0.064
P64[a]	D	(*i*Pr)$_2$-N-(CH$_2$)$_2$–	8.174	8.634	−0.460

(*continued on next page*)

Table 1 (*continued*)

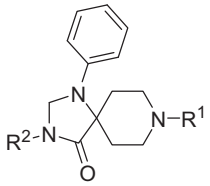

Compound	R1	A / R2	B	C	D	−log (K_i/nM)	
						Experimental	Predicted	Res
P65	D	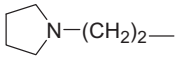				8.854	8.888	−0.034
P66[a]	D	$BuNH(CH_2)_2$–				9.301	9.171	0.130
P67	D	*i*-AmylNH$(CH_2)_2$–				9.398	9.251	0.147
P68	D	*c*-HexylCH_2NH$(CH_2)_2$–				9.155	9.212	−0.057
P69	D	BnNH$(CH_2)_2$–				8.444	8.382	0.062
P70	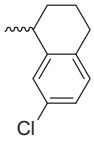	BuNH–				7.799	7.721	0.078
P71[a]	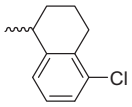	BuNH–				8.745	8.941	−0.196
P72	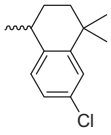	BuNH–				9.222	9.151	0.071
P73	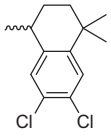	BuNH–				7.914	7.887	0.027

[a] Test set. Res = $pK_{i\ Experimental} - pK_{i\ Predicted}$.

compounds. The nitrogen atoms close to the R^1 group for those ligands are positively charged. And the compounds were minimized with a non-bond cut-off of 8 Å using Powell conjugate-gradient algorithm. The convergence criterion was set to 0.05 kcal/mol. The most active compound **P67** served as an alignment template for superposition.

Following the standard CoMFA procedure, each compound was mapped onto a 3D lattice with grid points 2.0 Å apart. An sp^3 carbon atom with +1 charge was employed to probe the steric (Lennard-Jones) and electrostatic (Coulombic) field energies. The cut-off interaction energies were set to 30 kcal/mol. Column filtering, for any column (lattice points) of computed molecular-field energies with a variance less than 2.0 kcal/mol, was applied to reduce computation time without negatively affecting the quality of the CoMFA models.

The robustness of the partial-least-squares (PLS) analysis embedded in CoMFA was addressed by internal cross-validation using the leave-one-out (LOO) procedure.[21–23] As an acceptable practice in 3D-QSAR studies, a cross-validated regression coefficient q^2 being higher than 0.5 can be considered as a statistical proof with high predictability,[22,23] while the conventional regression coefficient r^2 should be more than 0.9.

Four GPCRs, including human A2A Adenosine Receptor (3EML), Beta1-Adrenergic G Protein-Coupled Receptor (Protein code: 2VT4), Beta2-Adrenergic G Protein-Coupled Receptor (2RH1), and Rhodopsin (3DQB), were evaluated. Considering the sequence identity as well as some key residues (Supplementary data Appendix 1), the Beta2-Adrenergic G Protein-Coupled Receptor was selected as a template for the homology modeling. The sequences of the template and human ORL1-receptor (SwissProt P41146) were aligned using the sequence alignment protocol within Accelrys Discovery Studio 2.5.[24] The structure information predicted by the TRANSMEM method is considered in the alignment. NOP indicates a sequence identity of 24.6% to the template in

Table 2
Statistical parameters of the CoMFA models

Training set	
q^2	0.819
q^2_{LEO} (average of 30 runs)	0.795
r^2	0.950
SEE	0.179
F	160.1
Optimal components	6
Field fraction (%)	
S	57.0
E	43.0
Test set	
q^2	0.855
r^2	0.912
k	0.900

S = steric and *E* = electrostatic. *r*, *q*, *SEE*, and *F* are the conventional Pearson regression coefficient, cross-validated regression coefficient, standard error of estimate, and statistical *F* value, respectively. LEO means the leave-eight-out partial least-squares analysis. *k* is the slope of the linear regression for the test set.

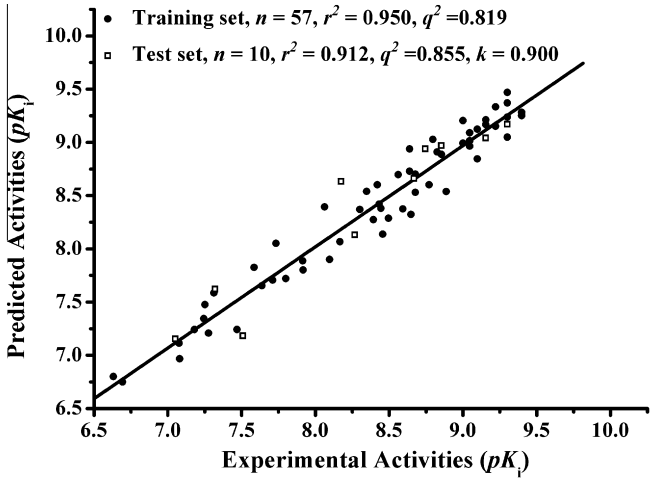

Figure 1. Plot of predicted versus experimental pK_i values of the 3D-QSAR CoMFA model.

Supplementary data Appendix 2. The model was built using the homology modeling protocol within Discovery Studio 2.5. A conserved disulfide bridge was formed based on the structure of the template (Fig. 3). The detailed parameters about the homology modeling method in the present study are given in Supplementary data Appendix 3.

The minimized NOP model was used for subsequent molecular docking simulation. Both Surflex-Dock and CDOCKER protocols[25–27] have been employed for the docking purpose in this study. The detailed parameters about the Surflex-Dock and CDOCKER methods in the present study are given in Supplementary data Appendix 4.

An excellent CoMFA model derived can account for the NOP binding affinities. The statistical parameters of the 3D-QSAR models are shown in Table 2. The LOO PLS analysis gives a relatively high q^2 value of 0.819 at six components, together with the conventional regression coefficient r^2 of 0.950 and a standard error of estimate of 0.195. The predicted pK_i values for each compound in the training set are given in Table 1 according to the best

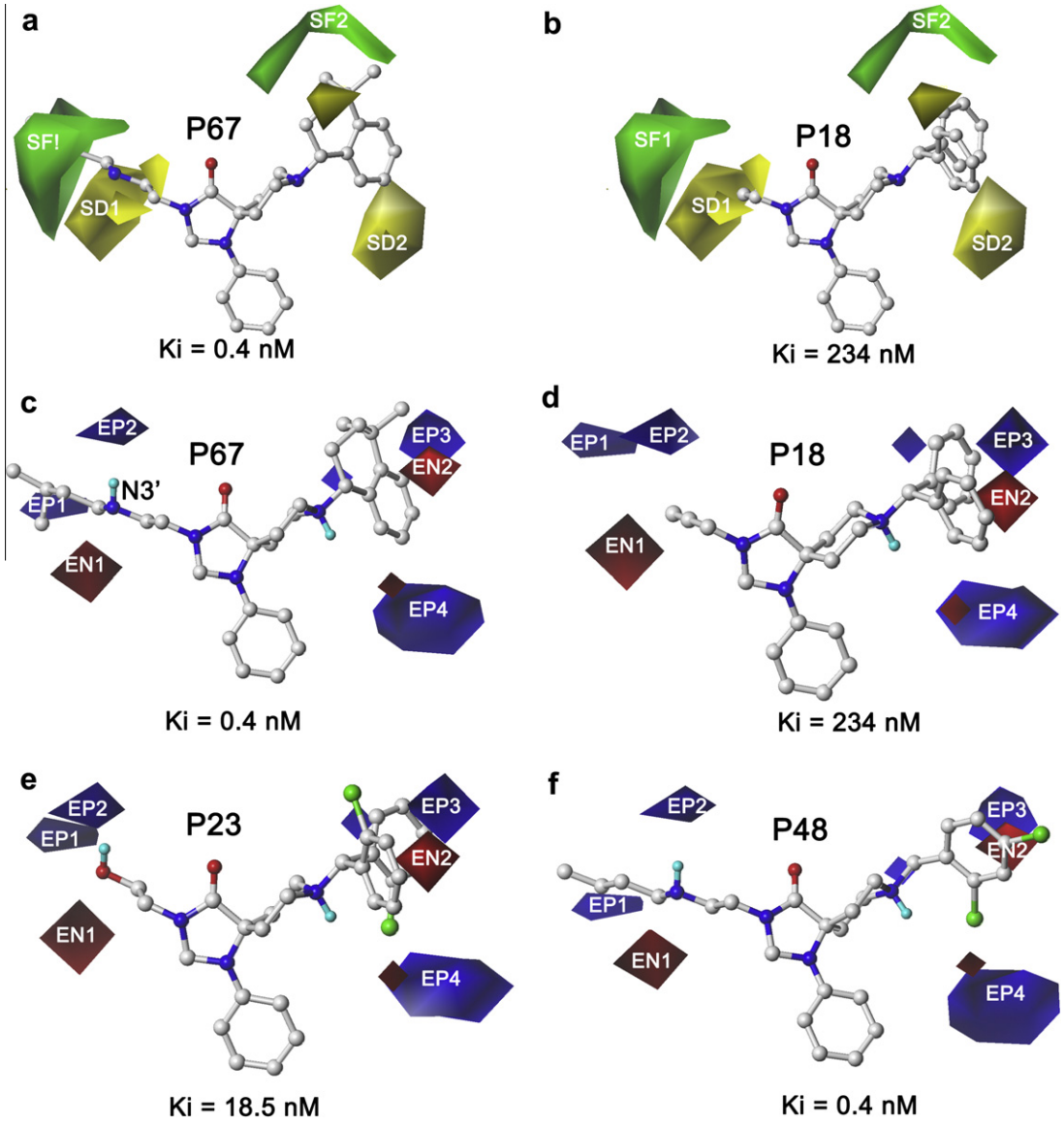

Figure 2. CoMFA contour maps: the steric/electrostatic maps for four compounds. In a and b, green (labeled as 'SF1' and 'SF2') and yellow ('SD1' and 'SD2') contours refer to the sterically favored (w.r.t. higher NOP binding affinity) and disfavored areas, respectively, while blue ('EP1', 'EP2', 'EP3', and 'EP4') and red ('EN1', and 'EN2') contours refer to regions where electropositive substituents are favorable and unfavorable in c, d, e, and f, respectively. Please refer to the web-version for the alternative color interpretation (nitrogen: blue; oxygen: red; and carbon: grey).

CoMFA model. Figure 1 shows a linear relationship between the CoMFA-predicted and experimental pK_i values for the training set. Linearity of the plots show very good correlations for the CoMFA model developed in the study for the NOP binding affinities of spiropiperidine analogues. The steric and electrostatic fields (at contributions 57.0% and 43.0% to the CoMFA model, respectively) are appropriate in interpreting the NOP binding affinities of the training set. Leave-eight-out cross-validation was also performed to estimate the extent of chance correlation in the CoMFA model. The mean (0.795) of the q^2 values from 30 runs, does not lead a different conclusion from that (0.819) of the LOO case.

The CoMFA model was not established by chance correlation. The affinity data for the training set were randomly shuffled and CoMFA models were rebuilt, which is so-called Y-Randomization. The statistical parameters (q^2 and r^2) of 30 newly derived models were compared with those of the original model. The CoMFA models in the Y-Randomization test yielded relatively poor statistical parameters (not shown), which further corroborate that the CoMFA model based on the original affinity data was not established by chance correlation.

The significance and predictability of QSAR models is generally checked by predicting the activity values of a set of compounds. An external test set is widely used to evaluate the predictability of a 3D-QSAR model. For a reliable and predictive model, the following criteria should be satisfied for the test set: $q^2 \geqslant 0.5$, $r^2 \geqslant 0.6$, and $0.85 \leqslant k \leqslant 1.15$. Herein, k refers to the slope of the regression line between the experimental and the predicted biological activities. An excellent correlation between the experimental and predicted biological activities is depicted in Figure 1 for the test set ($q^2 = 0.855$, $r^2 = 0.912$, and $k = 0.900$). The PLS regression coefficients (q^2 and r^2) and slope k of the regression line satisfied the recommended criteria.[22,23] The relatively high values of q^2 and r^2 confirm that the derived 3D-QASR/CoMFA model exhibits a good predictive ability in the external test-set validation.

3D contour maps were generated to display the correlation of experimental affinity data with changes in the steric/electrostatic molecular-field contributions, and aid in the rational design of novel and more effective NOP agonists. The steric properties of the CoMFA model are displayed in Figure 2a and b, while the electrostatic properties are displayed in Figure 2c and d. As demonstrated in Figure 2a, **P67** ($K_i = 0.4$ nM) orients its long alkyl chain to 'SF1'. The two methyls at the end of the chain enter the green areas, while another two methyls at the 4 position of the tetrahydronaphthalene ring are located near the 'SF2', which leads **P67** with relatively high affinity. Conversely, bulky groups close to the yellow contour 'SD1' result in a lower affinity. Accordingly, the propargyl group of **P18** (234 nM, the most inactive ligand, see Fig. 2b) and the allyl group of **P19** (203 nM) point toward the yellow isopleths. Compounds with bulky groups near the 'SD1' region (Supplementary data Appendix 5), such as **P29** (8.65 nM), **P30** (5 nM), and **P33** (12.1 nM), represent relatively lower NOP binding affinities comparing with those without bulky groups (**P27** 2.1 nM and **P28** 2.55 nM).

A secondary amine near the 3′ position of the alkyl chain will enhance affinity. The blue and red regions near the 3′ position of the alkyl chain of **P67** reveal the significance of arranging electropositive and electronegative groups at this position, which significantly influence affinity. For example, N at the 3′ position will enhance affinity. According to the MMFF94 partial atomic charge calculations, the carbon (0.00 |e|) at the 3 position of the butanyl chain in **P20** is replaced by nitrogen (−0.90 |e|) in **P26**. The only hydrogen (0.36 |e|) linked to the nitrogen in **P26** is close to the electropositively favorable region 'EP1', whereas the lone pair electrons of the nitrogen atom are adjacent to the electronegatively favorable area 'EN1'. As a result, higher affinity (4.05 nM) of the latter was observed than that (48.7 nM) of the former, as indicated in

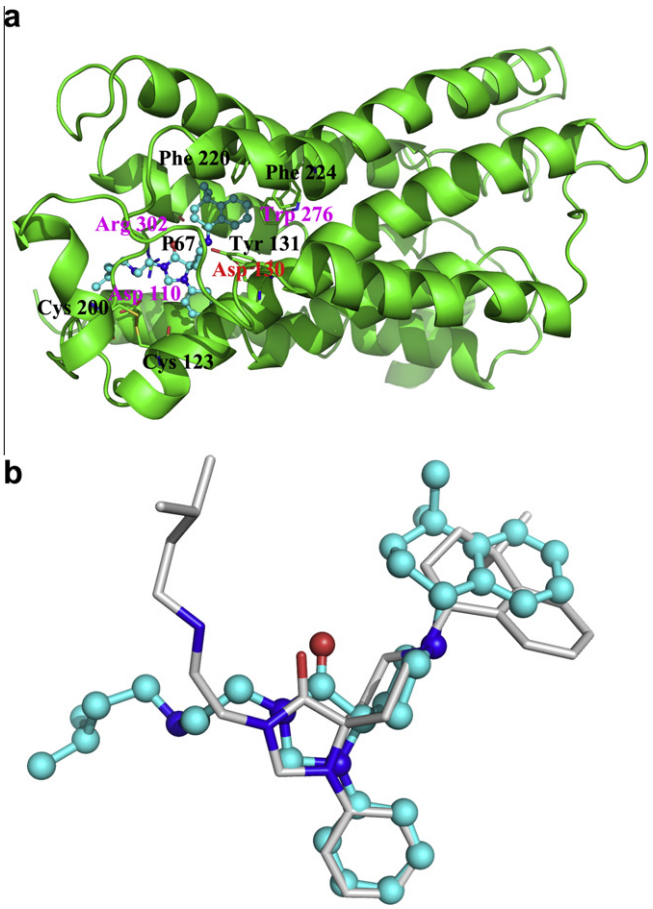

Figure 3. The docking-binding mode of the NOP (nociceptin/orphanin FQ receptor)/**P67** complex after molecular docking procedure. In (a), LHS: extracellular side and RHS: intracellular side, respectively. In (b), the docking pose obtained by Surflex-dock is shown in sticks, while the one obtained by CDOCKER is shown in CPK (nitrogen: blue; oxygen: red; and carbon: cyan/grey). Please refer to the web-version for the alternative color interpretation (nitrogen: blue; oxygen: red; and carbon: green/grey/cyan).

Supplementary data Appendix 5. In addition, the affinity of a compound with a secondary amine (**P48** 0.4 nM and **P43** 0.7 nM) is better than those with a primary/tertiary amine (**P25** 47.8 nM and **P64** 6.7 nM), which suggests an asymmetry electronic distribution. The reason for the ascending affinity order (**P20** and **P26)** can be used to account for the relatively higher affinities of **P48** and **P43** than those of **P25** and **P64**, respectively.

The R^1 substitute groups have a strong effect on activities. The biological activities of A-substituted and B-substituted compounds are relatively lower (23–234, 2.1–56 nM, respectively) than those of the C-substituted and D-substituted compounds (0.4–2.3, 0.4–5.4 nM, respectively). The contour map points out that the biphenyl-methyl group substituted at the 8th position decreases activity. In Figure 2d, blue contours 'EP3' are located above the plane of the upper phenyl of A, which cause energetically unfavorable repulsion and result in low activities. B-Substituted group is quite similar to A-substituted group, except that the chlorine substituted at the second position which has the electron-withdrawing effect to attenuate the electrostatic/steric repulsion with 'EP3'. Thus the activities of B-substituted compounds have a slightly boost than those of A-substituted counterparts when own the same R^2 functional groups. In comparison, the volumes of C-substituted and D-substituted groups are relatively smaller those of A-substituted and B-substituted groups, thus they reduce the energetically unfavorable repulsion with 'EP3' and lead relatively higher activities, which may explain why compounds **P28**, **P43**, and **P56** have

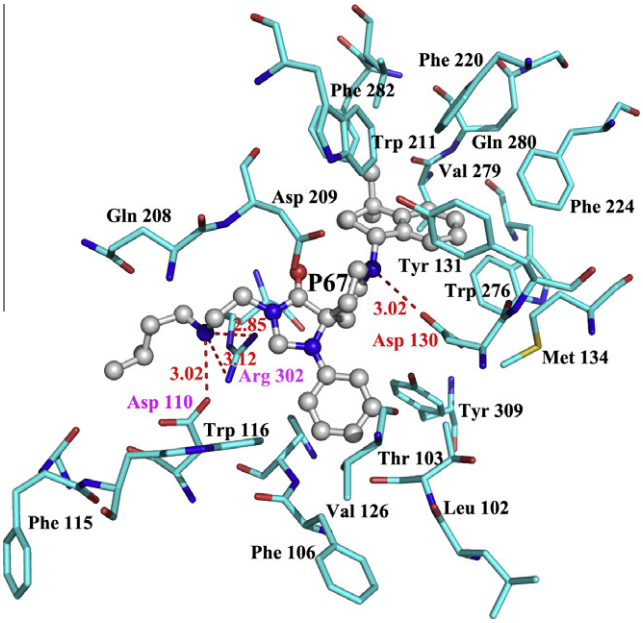

Figure 4. The docking-binding mode of **P67** in the active site of the nociceptin/orphanin FQ receptor obtained by CDOCKER. Hydrogen bonds are displayed in red dashes (Å). Please refer to the web-version for the alternative color interpretation (nitrogen: blue; oxygen: red; and carbon: cyan/grey).

different binding affinities although all of them contain the same *i*-PrNH$(CH_2)_2$– group. The similar trend could be applied to account for the affinity difference between **P34** and **P48**.

A 3D model of NOP built for the rational design of NOP agonists. The Ramachandran Plot of the 3D model is showed in Supplementary data Appendix 6, which is used to verify predicted torsion angles in proteins. It indicates low energy conformations for φ (phi) and ψ (psi), which are used to represent the torsion angles on either side of alpha carbons in peptides. In the plot, 97.6% residues locate in the preferred and allowed regions, whereas only 2.4% residues are in the disallowed regions. Besides, none of the residues within the binding pocket are in the disallowed regions, which corroborates the 3D model is acceptable for the molecular docking simulations and suitable for the structure-based molecular design of NOP agonists.

Salt bridge, hydrogen-bonding, and hydrophobic interactions can be identified as the underlying factors for the high NOP binding affinity of **P67.** The docking-binding mode of **P67** in the active site is shown in Figure 4. The protonated piperidine-nitrogen atom forms stable salt bridges with Asp130, which is a crucial anchoring point for agonists, as pointed out by site directed mutagenesis.[28,29] The D-substituted group takes up the hydrophobic pocket formed by Tyr131, Met134, Trp211, Phe220, Phe224, Trp276, Val279, and Val283. This hydrophobic pocket was proposed to hold the Phe1 sidechain of nociceptin (the endogenic agonist of NOP), and some of the residues (Tyr131, Phe220, Phe224, and Trp276), which are confirmed to have a significant effect on the binding by previous mutagenesis studies.[29,30] As described by N. Zaveri, there is a specific lipophilic area that triggers an agonist response when the site is occupied by an appropriately sized and placed lipophilic moiety.[30,31] Additionally, the long alkyl chain sketchs to another direction to form strong hydrogen bonds with Arg302 and Asp110 (**H1a** = 2.85 Å, **H1b** = 3.12 Å, and **H2** = 3.02 Å, respectively). The results are in agreement with the phenomenon that the secondary amine at the 3′ position enhances affinity. This nitrogen atom may work as a hydrogen donor when it interacts with Asp110, whereas serves as a hydrogen acceptor when it interacts with Arg302 (Asp 110 corresponds to 'EP2' and Arg302 refers to 'EN1'), which may explain the asymmetry electronic distribution in the 3D contour map (Fig. 2c). This result is also consistent with the previous works, which demonstrated that mutating Arg302 to a negative charged Asp would result in a great loss of nociceptin binding.[32] As a result, these energetically favorable interactions stabilize **P67** in the ligand-binding pocket.

In summary, the resulting CoMFA model performs well in both internal and external consistency in the present study. The excellent correlation between experimental and predicted pK_i values for the test set corroborated the predictive ability of the derived CoMFA model. Based on the 3D model of NOP built by homology modeling approach, molecular docking simulations reveal that several important residues (Asp110, Asp130, Tyr131, Typ276, and Arg302) exhibit salt bridge, hydrogen-bonding, and hydrophobic interactions with the most active agonist **P67**, which is consistent with the CoMFA contour maps and the experimental results from the literature.[19,30,31] The newly obtained 3D model of NOP may serve as a basis for the structure-based molecular design of novel agonists with enhanced affinity.

Our results highlight that the 3D-QSAR (ligand-based) and homology modeling/molecular docking (structure-based) approaches, which were integrated herein, would be useful for the exploratory study of some promising biological systems for drug discovery purpose with respect to affinity enhancement, especially for cases difficult to obtain the crystal structure of a potential protein.

Acknowledgments

The excellent suggestions from the anonymous reviewers are cordially appreciated. We cordially acknowledge the financial support from National Major Projects for science and technology development from Science and Technology Ministry of China (2009ZX09304-003), Fundamental Research Funds for the Central Universities (10ykjc20), Natural Science Foundation of Guangdong Province (9451008901001994), and Research Fund for the Doctoral Program of Higher Education of China (20090171120057).

Supplementary data

Supplementary data associated with this article can be found, in the online version, at doi:10.1016/j.bmcl.2010.09.116.

References and notes

1. Mollereau, C.; Parmentier, M.; Mailleux, P.; Butour, J. L.; Moisand, C.; Chalon, P.; Caput, D.; Vassart, G.; Meunier, J. C. *FEBS Lett.* **1994**, *341*, 33.
2. Waldhoer, M.; Bartlett, S. E.; Whistler, J. L. *Annu. Rev. Biochem.* **2004**, *73*, 953.
3. Meunier, J. C.; Mollereau, C.; Toll, L.; Suaudeau, C.; Moisand, C.; Alvinerie, P.; Butour, J. L.; Guillemot, J. C.; Ferrara, P.; Monsarrat, B., et al *Nature* **1995**, *377*, 532.
4. Reinscheid, R. K.; Nothacker, H.-P.; Bourson, A.; Ardati, A.; Henningsen, R. A.; Bunzow, J. R.; Grandy, D. K.; Langen, H.; Monsma, F. J., Jr.; Civelli, O. *Science* **1995**, *270*, 792.
5. Mogil, J. S.; Pasternak, G. W. *Pharmacol. Rev.* **2001**, *53*, 381.
6. Lambert, D. G. *Nat. Rev. Drug Disc.* **2008**, *7*, 694.
7. Chiou, L. C.; Liao, Y. Y.; Fan, P. C.; Kuo, P. H.; Wang, C. H.; Riemer, C.; Prinssen, E. P. *Curr. Drug Targets* **2007**, *8*, 117.
8. Christmas, D. M.; Hood, S. D. *Recent Pat. CNS Drug Discov.* **2006**, *1*, 289.
9. Jenck, F.; Moreau, J.-L.; Martin, J. R.; Kilpatrick, G. J.; Reinscheid, R. K.; Monsma, F. J.; Nothacker, H.-P.; Civelli, O. *Proc. Natl. Acad. Sci. U.S.A.* **1997**, *94*, 14854.
10. Gavioli, E. C.; Rae, G. A.; Calo, G.; Guerrini, R.; De Lima, T. C. M. *Br. J. Pharmacol.* **2002**, *136*, 764.
11. Jenck, F.; Wichmann, J.; Dautzenberg, F. M.; Moreau, J. L.; Ouagazzal, A. M.; Martin, J. R.; Lundstrom, K.; Cesura, A. M.; Poli, S. M.; Roever, S.; Kolczewski, S.; Adam, G.; Kilpatrick, G. *Proc. Natl. Acad. Sci. U.S.A.* **2000**, *97*, 4938.
12. Varty, G. B.; Hyde, L. A.; Hodgson, R. A.; Lu, S. X.; McCool, M. F.; Kazdoba, T. M.; Del Vecchio, R. A.; Guthrie, D. H.; Pond, A. J.; Grzelak, M. E.; Xu, X.; Korfmacher, W. A.; Tulshian, D.; Parker, E. M.; Higgins, G. A. *Psychopharmacology* **2005**, *182*, 132.

13. Varty, G. B.; Lu, S. X.; Morgan, C. A.; Cohen-Williams, M. E.; Hodgson, R. A.; Smith-Torhan, A.; Zhang, H.; Fawzi, A. B.; Graziano, M. P.; Ho, G. D.; Matasi, J.; Tulshian, D.; Coffin, V. L.; Carey, G. J. *J. Pharmacol. Exp. Ther.* **2008**, *326*, 672.
14. Hawes, B. E.; Graziano, M. P.; Lambert, D. G. *Peptides* **2000**, *21*, 961.
15. New, D. C.; Wong, Y. H. *Neurosignals* **2002**, *11*, 197.
16. Knoflach, F.; Reinscheid, R. K.; Civelli, O.; Kemp, J. A. *J. Neurosci.* **1996**, *16*, 6657.
17. Vaughan, C. W.; Christie, M. J. *Br. J. Pharmacol.* **1996**, *117*, 1609.
18. Caldwell, J. P.; Matasi, J. J.; Zhang, H.; Fawzi, A.; Tulshian, D. B. *Bioorg. Med. Chem. Lett.* **2007**, *17*, 2281.
19. Caldwell, J. P.; Matasi, J. J.; Fernandez, X.; McLeod, R. L.; Zhang, H. T.; Fawzi, A.; Tulshian, D. B. *Bioorg. Med. Chem. Lett.* **2009**, *19*, 1164.
20. Cherezov, V.; Rosenbaum, D. M.; Hanson, M. A.; Rasmussen, S. G. F.; Thian, F. S.; Kobilka, T. S.; Choi, H. J.; Kuhn, P.; Weis, W. I.; Kobilka, B. K.; Stevens, R. C. *Science* **2007**, *23*, 1258.
21. Sybyl Molecular Modeling Software Packages, V 7.3.5, TRIPOS Inc., St Louis, 2008.
22. Tropsha, A.; Gramatica, P.; Gombar, V. K. *QSAR Comb. Sci.* **2003**, *22*, 69.
23. Golbraikh, A.; Tropsha, A. *J. Mol. Graph. Model* **2002**, *20*, 269.
24. Discovery Studio 2.5, Accelrys Software Inc., San Diego, 2009.
25. Jain, Ajay N. *J. Comput. Aided. Mol. Des.* **2007**, *21*, 281.
26. Wu, G. S.; Robertson, D. H.; Brooks, C. L.; Vieth, M. *J. Comput. Chem.* **2003**, *24*, 1549.
27. Luo, H. –B.; Zheng, H.; Zimmerman, M. D.; Chruszcz, M.; Skarina, T.; Egorova, O.; Savchenkoc, A.; Edwardsc, A. M.; Minor, W. *J. Struct. Biol.* **2010**, *169*, 304.
28. Broer, B. M.; Gurrath, M.; Holtje, H. D. *J. Comput. Aided Mol. Des.* **2003**, *17*, 739.
29. Mouledous, L.; Topham, C. M.; Moisand, C.; Mollereau, C.; Meunier, J. C. *Mol. Pharmacol.* **2000**, *57*, 495.
30. Zaveri, N.; Jiang, F.; Olsen, C.; Polgar, W.; Toll, L. *AAPS J.* **2005**, *7*, E345.
31. Topham, C. M.; Mouledous, L.; Poda, G.; Maigret, B.; Meunier, J. C. *Protein Eng.* **1998**, *11*, 1163.
32. Kam, K. W. L.; New, D. C.; Wong, Y. H. *J. Neurochem.* **2002**, *83*, 1461.